Autonomic modulation of the electrical substrate in mice haploinsufficient for cardiac sodium channels: a model of the Brugada syndrome.

Malcolm Finlay[1], Justine Bhar-Amato[2], Keat-Eng Ng[1], Diogo Santos[2], Michele Orini[2], Vishal Vyas[1], Peter Taggart[2], Andrew A. Grace[3], Christopher L.-H. Huang[4], Pier D. Lambiase[2] & Andrew Tinker[1]

[1]William Harvey Research Institute, Barts and the London School of Medicine and Dentistry, Queen Mary University of London, London, UK

[2]Institute of Cardiovascular Science, University College London, London, UK

[3]Department of Biochemistry, University of Cambridge, Cambridge, United Kingdom

[4]Department of Physiology, Development and Neuroscience, University of Cambridge, Cambridge, United Kingdom

Running Title: Autonomic modulation of cardiac conduction velocity

Total Word Count: 5318

Address for Correspondence: Professor Andrew Tinker, William Harvey Heart Centre, Barts & The London School of Medicine & Dentistry, Charterhouse Square, London EC1M 6BQ. Tel: 020 7882 5783, E-mail: a.tinker@qmul.ac.uk

Abstract

A murine line haploinsufficient in the cardiac sodium channel has been used to model human Brugada syndrome: a disease causing sudden cardiac death due to lethal ventricular arrhythmias. We explored the effects of cholinergic tone on electrophysiological parameters in wild type and genetically modified, heterozygous, *Scn5a+/-* knockout mice. *Scn5a+/-* ventricular slices showed longer refractory periods than wild-type both at baseline and during isoprenaline challenge. *Scn5a+/-* hearts also showed lower conduction velocities and increased mean increase in delay than did littermate controls at baseline and blunted responses to isoprenaline challenge. Carbachol exerted limited effects but reversed the effects of isoprenaline with co-application. *Scn5a+/-* mice showed a reduction in conduction reserve in that isoprenaline no longer increased conduction velocity and this was not antagonised by muscarinic agonists.

Key Words: autonomic nervous system, conduction, *SCN5A* haploinsufficiency, Brugada syndrome

Abbreviations: MEA – multielectrode array, VERP – ventricular refractory period, *Scn5a+/-* – cardiac sodium channel (Scn5a) haploinsufficient mouse

Introduction

Brugada Syndrome is recognised by a triad of right bundle branch block, coved ST elevation in the right precordial leads and lethal ventricular arrhythmias (6; 25). It may be responsible for up to a fifth of cases of sudden cardiac death in the young (25). Where a mutation is identified this most commonly occurs in the main cardiac sodium channel isoform, SCN5A (4) though in many patients no obvious mutations are found. The main pathophysiological feature is the presence of significant cardiac conduction delays particularly in the right ventricular outflow tract and these contribute to the ECG pattern and arrhythmic predisposition (15). Furthermore, it is well known that sodium channel density is an important determinant of conduction velocity in the heart (14).

An interesting feature of Brugada Syndrome is that ventricular arrhythmia occurs at night when the patient is sleeping and this can be accompanied by accentuation of the characteristic ECG pattern (21; 23). The autonomic nervous system is well known to modulate ventricular excitability; however in many other channelopathies it is exercise or stress that precipitates ventricular tachycardia and/or fibrillation and thus this observation is intriguing (9). During rest, vagal activity is predominant in contrast to the situation in exercise where vagal activity is reduced and sympathetic drive predominates though the detailed picture may be more complex than this standard interpretation (18). In this study, we explore this question in a model of Brugada Syndrome namely the SCN5A- haploinsufficient mouse (*Scn5a*+/-). This model recapitulates a number of the features of Brugada syndrome seen in patients (11; 12; 19; 24) and provides a route to exploring the autonomic modulation of the electrophysiological substrate.

Methods

Murine breeding and genotyping

Mice were maintained in an animal core facility under UK Home Office guidelines relating to animal welfare. All mice were kept in individually ventilated, pathogen-free, temperature controlled cages (21-23ºC) with 12-hour day/night light cycles. Animals had free access to standard rodent chow and water. Mice of both sexes were studied between 12 and 24 weeks of age under standardized conditions for tissue slice analysis. Whole heart studies were performed at between 9 months and 1 year of age in mice of both sexes. The generation of the *Scn5a*+/- heterozygotic mice has been previously described (24). Genotyping was performed at 6 weeks of age. Littermate controls were used throughout, and experiments and analysis were performed blinded to genotype (MF, VV). The work was carried out under UK Home Office project licences PPL-6732 and PPL-7665.

Cardiac Excision

Mice were euthanized by cervical dislocation. The thorax was immediately dissected and the heart exposed. Cardioplegia was induced by applying 10 ml of ice-cold, oxygenated (bubbled with 95% O_2; 5% CO_2) Ca^{2+}-free Krebs solution (119 mM NaCl, 4 mM KCl, 1 mM $MgCl_2$, 1.2 mM KH_2PO_4, 25 mM $NaHCO_3$, 10 mM glucose, 2 mM Na pyruvate, pH 7.4) directly onto the epicardial surface. The heart and great vessels were removed within 20 sec and placed into a dissection dish containing oxygenated ice-cold Ca^{2+}-free Krebs solution. A 23 gauge cannula was inserted into the aorta and secured under light microscopy. For tissue slicing, cold retrograde perfusion was commenced with oxygenated, ice-cold, Ca^{2+} free Krebs solution at a flow rate of 16.5 ml/min. Whole-heart recording perfusion used oxygenated

Krebs solution (containing 1.4 mM Ca^{2+}) at room temperature. The time taken from cervical dislocation to establishment of Langendorff perfusion was less than 3 min.

Preparation of cardiac tissue slices

Following perfusion for 2 min, the perfusate was altered to an ice-cold oxygenated Ca^{2+}-free Krebs solution containing high K^+ (20 mM KCl) and blebbistatin (20 μM; Cambridge Bioscience, Cambs, UK) for 3 minutes. The hearts were then removed from the Langendorff perfusion rig and placed again in a dissection dish containing cold perfusate. Ventricular tissue was dissected from atrial tissue under light microscopy. The dissected ventricles were then embedded in low-melt agarose (4% low-melting point agarose in Ca^{2+}-free Krebs solution), and then rapidly chilled on ice. The agarose block was orientated and fixed onto a magnetic stage using cyanoacrylate glue and placed in the cutting chamber of a Vibratome (Campden Instruments, London, UK). This chamber was maintained at 4ºC using external ice. It was filled with cold, modified oxygenated Krebs solution (containing 0.6 mM Ca^{2+}, 10 mM K^+). Tissue sections were obtained from apex to base at an interval thickness of 200 μm. The vibrating PTFE-coated steel blade (Wilkinson Sword, Bucks, UK) was advanced at <200 μm/sec. The x-axis vibration was applied at an amplitude of 2 mm and frequency of 80 Hz. The z-axis deviation was calibrated prior to every use to be < 1μm. The cut sections were immediately placed in oxygenated low-Ca^{2+} Krebs solution (4 mM KCl, 0.6 mM Ca^{2+}) containing 10 mM blebbistatin maintained at room temperature. After 25 minutes, the samples were transferred to standard oxygenated Krebs solution (4 mM KCl, 1.1 mM Ca^{2+}) and kept at room temperature until electrophysiological studies were performed.

Cardiac slice electrophysiological (EP) studies

Stimulation was generated by a stimulus isolation unit (DS-2A, Warner Instruments, MA, USA) with signal timing driven by an Arduino Uno microcontroller (Arduino, It). Stimulation was applied using a silver chloride bipolar electrode. The sections were placed in the recording chamber and carefully positioned manually so that left ventricular tissue overlaid the measurement electrodes. A 1 cm diameter metal ring with an overlying nylon mesh (Harp-slice grid, Micro Control Instruments, East Sussex, UK) was used to hold the tissue flat in place on the electrode grid and ensured adequate tissue electrode contact. The recording chamber was mounted in the headstage and perfusion commenced at 2 ml/min. Tissue was allowed to settle to a steady state over 1 min before electrode placement. The bipolar stimulating electrode was carefully lowered to just contact the tissue slice on the left ventricular tissue, but not to move the slice on the array. Stimulation was started at a frequency of 5 Hz using a monophasic 1 ms duration pulse, for real-time recording of electrical activity. The stimulus voltage was increased until electrical capture was achieved. The stimulus voltage was then reduced until electrical capture was lost: the lowest voltage stimulus that could reliably achieve capture was then taken as the stimulus threshold. Cardiac signals were recorded at a sampling frequency of 10 kHz. A simulation protocol was performed with steady state pacing at an interstimulus interval of 200 ms, with stimulation during recording applied at an amplitude of twice threshold. Around 30 sec of pacing activity were recorded for each state for each slice. Perfusate solution containing drugs was washed in over 30 seconds at 20 ml/min. Slices were then stimulated at 5 Hz for 2 min before threshold was determined and recording commenced.

Ex-vivo whole heart recordings

For whole heart recordings, hearts were retrogradely perfused at 16.5 ml/min with normal oxygenated Krebs solution (Ca^{2+} 1.4 mM). A unipolar silver chloride stimulation

electrode and flexible 32-pole multi-electrode array (MEA) (FlexMEA, Multielectrode Systems) were placed on the ventricular epicardium and an S_1S_2 decremental stimulation protocol was performed to determine the ventricular effective refractory period (VERP). Stimulation was performed with a biphasic pulse of amplitude 2 V and duration 0.5 ms, with S_1S_2 intervals reduced from 150 ms by decrements of 5 ms to 100 ms and thereafter by decrements of 2 ms until tissue refractoriness was reached. Arrhythmogenicity was further tested for by applying stimulating trains of 100 beats at coupling intervals progressively reduced from 100 ms. Ventricular tachycardia was defined as a ventricular arrhythmia persisting more than 2 sec.

Analysis of electrograms

All analysis of murine electrophysiology was performed using custom software running in Matlab, v2014b (The Mathworks Inc., MA, USA). The time point of local activation was taken at the steepest negative gradient of the unipolar electrogram. Conduction velocities were determined using a gradient method, with conduction velocity defined as the inverse of the gradient in activation times across the array (Figure 1A-C). Electrodes with significant noise were excluded, and all electrograms and time points were checked manually. Mean increase in delay (MID), a well-validated measure of inducibility of conduction delay, was calculated by determining the area under the conduction-delay curve (15) and according to the equation

$$MID = \frac{\left(\int_{minS2\ CI}^{S1\ CI}(Activation\ Time - Activation\ Time\ at\ S1CI)\right)}{S1\ CI - minS2\ CI}$$

Where MID is Mean Increase in Delay, S1 CI is the coupling interval of steady state pacing (S1) and minS2 CI is the minimum coupling interval above ERP. The integral was calculated using the trapz function in Matlab.

The mean timing of the activation time of all recording electrodes was used for each measurement of conduction delay, and the MID defined as the unit increase in conduction delay per unit reduction in S_1S_2 coupling interval (ms/ms). Stimulation protocols were performed in normal Kreb's solution, in baseline (control) conditions or with isoprenaline 100 nM and/or carbachol 10 μM.

Immunofluorescence of cardiac sections

Mouse hearts were rinsed in PBS and cut longitudinally with a blade and tissue holder. The hearts were fixed in 10% formalin (Sigma) for at least 24 hours followed by two PBS washes and stored in 70% ethanol before paraffin embedding. Paraffin-embedded hearts were cut to 5 μm thick sections and mounted on Superfrost plus microscope slides. Sections were then deparaffinized with xylene and rehydrated with 4 ethanol washes (from 100%-50%) before heat-mediated antigen retrieval with citrate buffer (pH 6.0). Following antigen retrieval, sections were washed several times in PBS, permeabilized with 0.1% Triton X-100 for 15 minutes and blocked with 5% goat serum in PBS for 1 hour at room temperature. Sections were then incubated with primary antibodies with 1% goat serum overnight at 4°C: Mouse monoclonal Cx43 clone 4E6.2 (Millipore MAB3067) and rabbit polyclonal N cadherin antibody (Santa Cruz SC-7939). The sections were incubated with fluorescently labelled secondary antibodies Alexa Fluor goat anti-mouse 488 and goat anti-rabbit 555 secondary antibodies (Invitrogen, UK) for 1 hour at room temperature in the dark. Sections were washed several times with PBS and co-stained with DAPI (nuclear stain) and stored in the dark until further analysis. The samples were analyzed using confocal microscopy (LSM

510, Carl Zeiss with DAPI: Excitation 405 nm, Emission LP420, FITC: Excitation 488 nm, Emission BP 505-550 and Cy3: Excitation 543 nm, Emission LP 560. Images were acquired sequentially. Quantitative analysis of the images was performed using ImageJ. Thresholding was applied to the images and they were then converted to binary files. The Cx43 stained image was subtracted by the N-cadherin stained image and represented "Cx43 not located at the intercalated disk".

Statistical analysis

All statistical analysis was performed using R software (The Comprehensive R Archive Network (CRAN)). Continuous parametric data are presented as means ± standard deviations (SD) or, in the case of significance derived from regression models, mean with [95% confidence interval], unless otherwise specified. Comparisons in which a single measurement was taken for each subject, e.g. ventricular effective refractory period (VERP), dispersion of repolarisation time, were made using Student's t-test with post-hoc correction for multiple comparisons. Continuous parametric data derived from electrogram data were modelled using mixed-effects linear regression (software: Linear and Nonlinear Mixed Effects (NLME) package running in R version 2.14) and statistical significance was inferred from the model. Quartile regression with bootstrapping (Quantile Regression Description Estimation and inference (QUANTREG) package) was used to compare non-parametric continuous data. Statistical significance is indicated by *$p<0.05$, **$p<0.01$ and ***$p<0.001$.

Results

There are conflicting reports of the effects of autonomic modulation on electrophysiological parameters in ventricular tissue such as conduction velocity (7). We accordingly investigated the effects of autonomic challenge on indices representing activation and recovery in littermate normal murine hearts and *Scn5a*-haploinsufficient heterozygous (*Scn5a*+/-) mice. We used two approaches to examine tissue level electrophysiology: tissue slices from juvenile animals (aged 2-3 months) placed on a MEA system, and *ex*-vivo Langendorff perfused hearts from mature animals (aged 9 months to a year) studied using an externally applied electrode array. Previous studies in older Langendorff perfused hearts had associated arrhythmic phenotypes with the *Scn5a*+/- genotype but we were unable to obtain viable tissue slices from older animals for multi-electrode array studies. We applied isoprenaline as a β-adrenoreceptor activator to mimic sympathetic activation and the muscarinic receptor agonist carbachol, to approximate vagal activation.

Ventricular slices obtained from juvenile *Scn5a*+/- mice required higher stimulus voltages than did wildtype (4.0 ± 0.7 vs 2.7 ± 0.4 V at baseline, **) for consistent capture, both before, and following all the different pharmacological manipulations. Untreated slices from *Scn5a*+/- hearts showed a trend towards lower conduction velocities than WT hearts (0.31 ± 0.04 vs 0.40 ± 0.7 m/s), but this was not statistically significant. Isoprenaline (100 nM) challenge increased conduction velocity in slices from wildtype (0.58 ± 0.11 m/s) but not in *Scn5a*+/- heart slices (0.34 ± 0.05 m/s) *. The increase in conduction velocity was reversed with carbachol co-application (Figure 2). Tissue slices from *Scn5a*+/- hearts showed consistently longer effective refractory periods both before (means ± SEM: *Scn5a*+/- 79 ± 4 vs WT 63 ± 4 ms, ***) and during isoprenaline challenge (73 ± 7 vs 52 ± 7 ms). Carbachol

markedly shortened the VERP in slices from WT but not *Scn5a+/-* hearts (Scn5a+/-: 76±7 ms, WT: 41±5 ms **).

In Langendorff-perfused isolated hearts, S_1S_2 decremental protocols were attempted before pharmacological challenge, and in the presence of isoprenaline 100 nM, and/or carbachol 10 μM. However, pacing capture became inconsistent during carbachol administration in 6 out of 8 *Scn5a+/-* hearts, despite attempts at increasing stimulation amplitude. Data from Langendorff-perfused *Scn5a+/-* hearts were therefore formally analysed for isoprenaline effects only (n=11) and were compared to littermate WT hearts (n=10). Washout (5 mins) was performed between drug challenges. *Scn5a+/-* hearts showed blunted responses to isoprenaline, mimicking the data from the cardiac tissue slice preparations (Figure 3). Notably, a 16% increase in conduction velocity observed in WT hearts in response to isoprenaline was again blunted in *Scn5a+/-* hearts (normalised conduction velocity control vs *Scn5a -/-* response to isoprenaline **), which exhibited a marginal decrease in conduction velocity. No consistent changes in electrophysiological parameters were observed during carbachol administration in the WT group.

Induced conduction delay in response to premature extrastimuli was also investigated. Mean increase in delay was almost double in *Scn5a+/-* hearts compared to WT controls (***). Controls and *Scn5a+/-* murine hearts studied through these procedures did not show differences in arrhythmia inducibility under control conditions, or isoprenaline 100 nM or carbachol 10 μM challenge (arrhythmic phenomena shown in 1/7 hearts in both drug challenges, with no sustained arrhythmias in either *Scn5a -/+* or controls). Little consistent change in VERP with drug challenge was observed in whole heart preparations (Figure 3C).

Finally we investigated a possible relationship between haploinsufficiency of Scn5a and the localization and expression of Cx43 in the juvenile animals. The expression of Cx43 was not grossly changed but there was an impression of localisation away from the

intercalated disc (marked by N-Cadherin staining) and into the cytosol (Figure 4). We confirmed this by quantifying the redistribution as detailed in the Methods. We expressed the localisation as a ratio of the amount of Cx43 not at the intercalated divided by the total expression of Cx43. In wildtype mice this number was 53.7 ± 3.9% and in *Scn5a*+/- mice 71.6% ± 2.7% (n=5 both groups, $P<0.01$).

Discussion

In this study we have investigated the tissue level electrophysiological properties of ventricles from *Scn5a* haploinsufficient mice and compared these to littermate controls. Our main finding is that there is an impairment of the response of conduction velocity to autonomic challenge in *Scn5a+/-* mice. In hearts from control mice, isoproterenol increased conduction velocity and decreased mean propagation delays. *Scn5a+/-* hearts demonstrated a reduced response of conduction velocity with increased mean propagation delays in response to isoprenaline. This effect was reversed by further challenge with carbachol, a muscarinic agonist although carbachol alone did not have prominent effects. This is consistent with previous reports that sympathetic activation increases conduction velocity in normal hearts (2; 7). In heart slice preparations in juvenile animals, ERP was prolonged in *Scn5a+/-* hearts whilst in older animals there was no significant difference when studied in Langendorff perfused intact hearts.

The findings in murine hearts may correlate with previous reports that β-adrenoreceptor activation increases sodium currents and therefore action potential conduction velocity through a protein kinase A dependent mechanism (20); reduced effects of isoprenaline could then be associated with the Na^+ channel haploinsufficiency in *Scn5a+/-* hearts. There is also the possibility that signalling pathways downstream of the β- adrenergic signalling pathway may also modulate gap junction density at the intercalated disc (7; 16). We also saw a potential mislocalization of Cx43 away from the intercalated disk in sodium channel haploinsufficient mice and this may contribute to the conduction slowing. It is plausible that some form of interaction with scaffolding or other proteins may be responsible for maintaining stoichiometry of Cx43 and Scn5a at the intercalated disk. A number of interacting sodium channel proteins are known and Cx43 can influence the trafficking of Scn5a (1; 27). This is a topic for investigation in future studies. We did not see prominent

responses to carbachol in tissue level electrophysiological parameters after washout of isoprenaline. However, combined application of both isoprenaline and carbachol in wildtype tissue slices reversed the effect of isoprenaline on conduction velocity. This likely involves receptor activation of M_2 muscarinic receptors coupled to inhibitory G-proteins that directly antagonise the response at the level of adenylate cyclase (10). The G_{i2} isoform seems to be central to muscarinic receptor signalling: L-type calcium channel modulation in ventricular myocytes is known to be abolished in G_{i2} knockout mice (8). The slow conduction may be pro-arrhythmic through promotion of re-entry and wavebreak. Importantly, the increases in MID observed in *Scn5a+/-* hearts provide evidence of the propensity for this group to have greater induced (rather than fixed) conduction velocity slowing. The implication therefore is that the consistency of conduction may become destablised when challenged by premature extrastimuli in the context of autonomic modulation; whilst in the steady-state or resting condition these hearts exhibit conduction velocity dynamics similar to those in wild-type littermates.

The marked differences in baseline conduction velocities between the tissue slice preparations and the whole heart Langendorff preparations may result from the involved tissue preparation techniques required to obtain viable slices. Even limited tissue disruptions that may have occurred during slice preparation could lead to reductions in cell-to-cell coupling, and thus accentuate pre-existing conduction delays.

In understanding the human Brugada syndrome two main hypotheses have been advanced (3; 15; 22): either that conduction is slowed and thus activation delayed or that repolarisation occurs prematurely. More specifically, coved ST segment elevation in ECG leads V1-V3, often taken as the hallmark of the syndrome, equates to either delayed depolarisation from the RV body to the RVOT or a shortened action potential in the epicardium leading to repolarisation gradients across the right ventricular wall. The present

findings in this mouse model show that autonomic activation has the potential to significantly modulate conduction delays, particularly in the context of pre-existing conduction deficiency. Our major finding is that adrenergic increases in conduction velocity are impaired in the *Scn5a+/-* mouse. This process in the normal murine heart is antagonised by muscarinic receptor activation but lost in the sodium channel haploinsufficient mouse. In the intact animal there will be a degree of autonomic balance and even at rest vagal tone will be modified by a degree of sympathetic drive. The absolute slowing may then be greatest when high vagal tone is combined with cardiac sodium channel haploinsufficiency. We have recently completed a study in man examining the effects of edrophonium on endocardial and epicardial right ventricular electrophysiology (5). We demonstrated that edrophonium appears to modulate both conduction and repolarisation in patients with BrS, particularly delaying activation and repolarisation in the right ventricular epicardium, in line with these presented results.

Though the use of isolated tissue from transgenic mice permits study of tissue-level phenomena, this approach does have limitations which are reflected in this study. The relatively small anatomy and thin ventricular walls did not permit detailed examination of differential epicardial and endocardial characteristics or selective studies of the right ventricular outflow tract. However with some adaptation of the array technology this may be possible in the future. In a previous study, only a trend to an increase in conduction velocity with isoprenaline was observed which did not reach statistical significance. (17). Variations in animal lines may explain such variance. Sodium channel mutations leading to phenotypic disease can occur in families where BrS is inherited in an autosomal dominant fashion. In general these mutations lead to a loss of sodium channel function and the disease is generated by *SCN5A* haploinsufficiency (13; 26). However in the majority of patients no mutation is obvious, the disease occurs sporadically and may have a different pathogenesis (13; 26).

Caution must therefore be exercised in applying the results of animal studies to this human syndrome.

In conclusion we have examined the influence of autonomic regulation on tissue level cardiac electrophysiology in a mouse model of BrS. Haploinsufficiency of *Scn5a* leads to impairment of conduction velocity reserve with blunting of sympathetically mediated increases and reversal by muscarinic receptor activation compared to littermate control mice.

Acknowledgements

JBA was funded by a Heart Research UK Fellowship, MO is funded by a Marie Curie Fellowship, DS funded by an MRC CASE Studentship, PDL is supported by UCLH Biomedicine NIHR, Barts BRC & Stephen Lyness Memorial Fund & CLHH is funded by the British Heart Foundation. AT is supported by the British Heart Foundation (RG/15/15/31742). AT and MF were facilitated in this project by the NIHR Biomedical Research Centre at Barts. The authors have no conflicts of interest.

Figure Legends

Figure 1. Measurement of conduction velocity and Mean Increase in Delay from multielectrode array. A. An example electrogram from a single electrode of a multielectrode array is shown. The local activation time is taken as the dV/dt min(arrow), during calculation the pacing artefact is blanked. **B**. Each electrogram and activation time is assigned to a 2D coordinate on a grid reflecting the geometry of the multielectrode array. Local activation time is determined for all the electrodes on the grid. Electrode numbers are given as E1, E2 etc. **C.** The gradient of activation times is then determined by interpolation (shown as a colourmap). The inverse of this "activation time gradient" can be determined to give the conduction velocity. The median conduction velocity over the multielectrode array was used for measurement. **D.** Determination of Mean Increase in Delay. The activation time is plotted for a series of S1S2 coupling intervals. The mean change in activation time over this interval (the Mean Increase in Delay, MID) is calculated by determining the area of the activation time change with coupling interval change (shaded area in figure). This area is divided by the Change in Coupling Interval to give the unit Mean Increase in Delay. The MID allows the susceptibility to conduction slowing with coupling interval changes to be compared.

Figure 2. Murine tissue slice conduction velocity (CV) measurements. A. Light microscope image of ventricular slice section on multielectrode array. B. Example electrograms acquired from WT and *Scn5a*+/- mice hearts under baseline and isoprenaline challenge. C. The effects of isoprenaline (Iso) and the ACh agonist carbachol (Carb) are shown in the 2 murine groups. A significant increase in CV is seen in response to isoprenaline which is absent in the Scn5a+/- mice. This effect is abolished by carbachol. Asterisks indicate

statistical significances from comparisons between Scn5a+/- and wild type (** p<0.01, ***p<0.001).

Figure 3. Electrophysiological properties of Langendorff-perfused hearts from *Scn5a*+/- and wild type mice under isoprenaline challenge. A. Conduction velocity dynamics mirrored those seen in tissue slice preparations, with paradoxical responses to isoprenaline challenge in the heterozygous mouse hearts. The MID of Scn5a+/- hearts was markedly greater than those of WT animals (B). Unlike tissue slices, only marginal differences in ERP were observed in whole heart preparations (C). Asterisks indicate statistical significances from comparisons between Scn5a+/- and wild type (** p<0.01, ***p<0.001).

Figure 4. The localisation of Cx43 in *Scn5a*+/- and wild type mice using laser scanning confocal microscopy. Representative heart sections are shown with N-cadherin staining marking the intercalated disc and DAPI the nucleus. Cx43 is expressed and present at the intercalated disc however there is an impression of mislocalisation of Cx43 away from the intercalated disc. This is confirmed using a numerical approach as detailed in the text. The sections are representative of a number of sections from a single mouse and the experiment was repeated in an additional littermate control and *Scn5a*+/- mouse (n=5 total sections in each group).

Reference List

1. **Agullo-Pascual E, Lin X, Leo-Macias A, Zhang M, Liang FX, Li Z, Pfenniger A, Lubkemeier I, Keegan S, Fenyo D, Willecke K, Rothenberg E and Delmar M**. Super-resolution imaging reveals that loss of the C-terminus of connexin43 limits microtubule plus-end capture and NaV1.5 localization at the intercalated disc. *Cardiovasc Res* 104: 371-381, 2014.

2. **Ajijola OA, Lux RL, Khahera A, Kwon O, Aliotta E, Ennis DB, Fishbein MC, Ardell JL and Shivkumar K**. Sympathetic modulation of electrical activation in normal and infarcted myocardium: implications for arrhythmogenesis. *Am J Physiol Heart Circ Physiol* 312: H608-H621, 2017.

3. **Antzelevitch C**. Genetic, molecular and cellular mechanisms underlying the J wave syndromes. *Circ J* 76: 1054-1065, 2012.

4. **Bezzina CR, Lahrouchi N and Priori SG**. Genetics of sudden cardiac death. *Circ Res* 116: 1919-1936, 2015.

5. **Bhar-Amato J, Finlay M, Santos D, Orini M, Chaubey S, Vyas V, Taggart P, Grace AA, Huang CL, Ben SR, Tinker A and Lambiase PD**. Pharmacological Modulation of Right Ventricular Endocardial-Epicardial Gradients in Brugada Syndrome. *Circ Arrhythm Electrophysiol* 11: e006330, 2018.

6. **Brugada P and Brugada J**. Right bundle branch block, persistent ST segment elevation and sudden cardiac death: a distinct clinical and electrocardiographic syndrome. A multicenter report. *J Am Coll Cardiol* 20: 1391-1396, 1992.

7. **Campbell AS, Johnstone SR, Baillie GS and Smith G**. beta-Adrenergic modulation of myocardial conduction velocity: Connexins vs. sodium current. *J Mol Cell Cardiol* 77: 147-154, 2014.

8. **Chen F, Spicher K, Jiang M, Birnbaumer L and Wetzel GT**. Lack of muscarinic regulation of Ca(2+) channels in G(i2)alpha gene knockout mouse hearts. *Am J Physiol Heart Circ Physiol* 280: H1989-H1995, 2001.

9. **Finlay M, Harmer SC and Tinker A**. The control of cardiac ventricular excitability by autonomic pathways. *Pharmacol Ther* 174: 97-111, 2017.

10. **Gomeza J, Zhang L, Kostenis E, Felder CC, Bymaster FP, Brodkin J, Shannon H, Xia B, Duttaroy A, Deng CX and Wess J**. Generation and pharmacological analysis of M2 and M4 muscarinic receptor knockout mice. *Life Sci* 68: 2457-2466, 2001.

11. **Jeevaratnam K, Guzadhur L, Goh YM, Grace AA and Huang CL**. Sodium channel haploinsufficiency and structural change in ventricular arrhythmogenesis. *Acta Physiol (Oxf)* 216: 186-202, 2016.

12. **Jeevaratnam K, Poh TS, Zhang Y, Rewbury R, Guzadhur L, Duehmke R, Grace AA, Lei M and Huang CL**. Delayed conduction and its implications in murine

Scn5a(+/-) hearts: independent and interacting effects of genotype, age, and sex. *Pflugers Arch* 461: 29-44, 2011.

13. **Kapplinger JD, Tester DJ, Alders M, Benito B, Berthet M, Brugada J, Brugada P, Fressart V, Guerchicoff A, Harris-Kerr C, Kamakura S, Kyndt F, Koopmann TT, Miyamoto Y, Pfeiffer R, Pollevick GD, Probst V, Zumhagen S, Vatta M, Towbin JA, Shimizu W, Schulze-Bahr E, Antzelevitch C, Salisbury BA, Guicheney P, Wilde AA, Brugada R, Schott JJ and Ackerman MJ**. An international compendium of mutations in the SCN5A-encoded cardiac sodium channel in patients referred for Brugada syndrome genetic testing. *Heart Rhythm* 7: 33-46, 2010.

14. **King JH, Huang CL and Fraser JA**. Determinants of myocardial conduction velocity: implications for arrhythmogenesis. *Front Physiol* 4: 154, 2013.

15. **Lambiase PD, Ahmed AK, Ciaccio EJ, Brugada R, Lizotte E, Chaubey S, Ben-Simon R, Chow AW, Lowe MD and McKenna WJ**. High-density substrate mapping in Brugada syndrome: combined role of conduction and repolarization heterogeneities in arrhythmogenesis. *Circulation* 120: 106-4, 2009.

16. **Lambiase PD and Tinker A**. Connexins in the heart. *Cell Tissue Res* 360: 675-684, 2015.

17. **Lane JD, Montaigne D and Tinker A**. Tissue-Level Cardiac Electrophysiology Studied in Murine Myocardium Using a Microelectrode Array: Autonomic and Thermal Modulation. *J Membr Biol* 250: 471-481, 2017.

18. **Machhada A, Trapp S, Marina N, Stephens RCM, Whittle J, Lythgoe MF, Kasparov S, Ackland GL and Gourine AV**. Vagal determinants of exercise capacity. *Nat Commun* 8: 15097, 2017.

19. **Martin CA, Siedlecka U, Kemmerich K, Lawrence J, Cartledge J, Guzadhur L, Brice N, Grace AA, Schwiening C, Terracciano CM and Huang CL**. Reduced Na(+) and higher K(+) channel expression and function contribute to right ventricular origin of arrhythmias in Scn5a+/- mice. *Open Biol* 2: 120072, 2012.

20. **Matsuda JJ, Lee H and Shibata EF**. Enhancement of rabbit cardiac sodium channels by beta-adrenergic stimulation. *Circ Res* 70: 199-207, 1992.

21. **Matsuo K, Kurita T, Inagaki M, Kakishita M, Aihara N, Shimizu W, Taguchi A, Suyama K, Kamakura S and Shimomura K**. The circadian pattern of the development of ventricular fibrillation in patients with Brugada syndrome. *Eur Heart J* 20: 465-470, 1999.

22. **Meregalli PG, Wilde AA and Tan HL**. Pathophysiological mechanisms of Brugada syndrome: depolarization disorder, repolarization disorder, or more? *Cardiovasc Res* 67: 367-378, 2005.

23. **Mizumaki K, Fujiki A, Tsuneda T, Sakabe M, Nishida K, Sugao M and Inoue H**. Vagal activity modulates spontaneous augmentation of ST elevation in the daily life of patients with Brugada syndrome. *J Cardiovasc Electrophysiol* 15: 667-673, 2004.

24. **Papadatos GA, Wallerstein PM, Head CE, Ratcliff R, Brady PA, Benndorf K, Saumarez RC, Trezise AE, Huang CL, Vandenberg JI, Colledge WH and Grace AA**. Slowed conduction and ventricular tachycardia after targeted disruption of the cardiac sodium channel gene Scn5a. *Proc Natl Acad Sci U S A* 99: 6210-6215, 2002.

25. **Priori SG, Wilde AA, Horie M, Cho Y, Behr ER, Berul C, Blom N, Brugada J, Chiang CE, Huikuri H, Kannankeril P, Krahn A, Leenhardt A, Moss A, Schwartz PJ, Shimizu W, Tomaselli G, Tracy C, Ackerman M, Belhassen B, Estes NA, III, Fatkin D, Kalman J, Kaufman E, Kirchhof P, Schulze-Bahr E, Wolpert C, Vohra J, Refaat M, Etheridge SP, Campbell RM, Martin ET and Quek SC**. Executive summary: HRS/EHRA/APHRS expert consensus statement on the diagnosis and management of patients with inherited primary arrhythmia syndromes. *Europace* 15: 1389-1406, 2013.

26. **Sarquella-Brugada G, Campuzano O, Arbelo E, Brugada J and Brugada R**. Brugada syndrome: clinical and genetic findings. *Genet Med* 18: 3-12, 2016.

27. **Shy D, Gillet L and Abriel H**. Cardiac sodium channel NaV1.5 distribution in myocytes via interacting proteins: the multiple pool model. *Biochim Biophys Acta* 1833: 886-894, 2013.

Figure 1

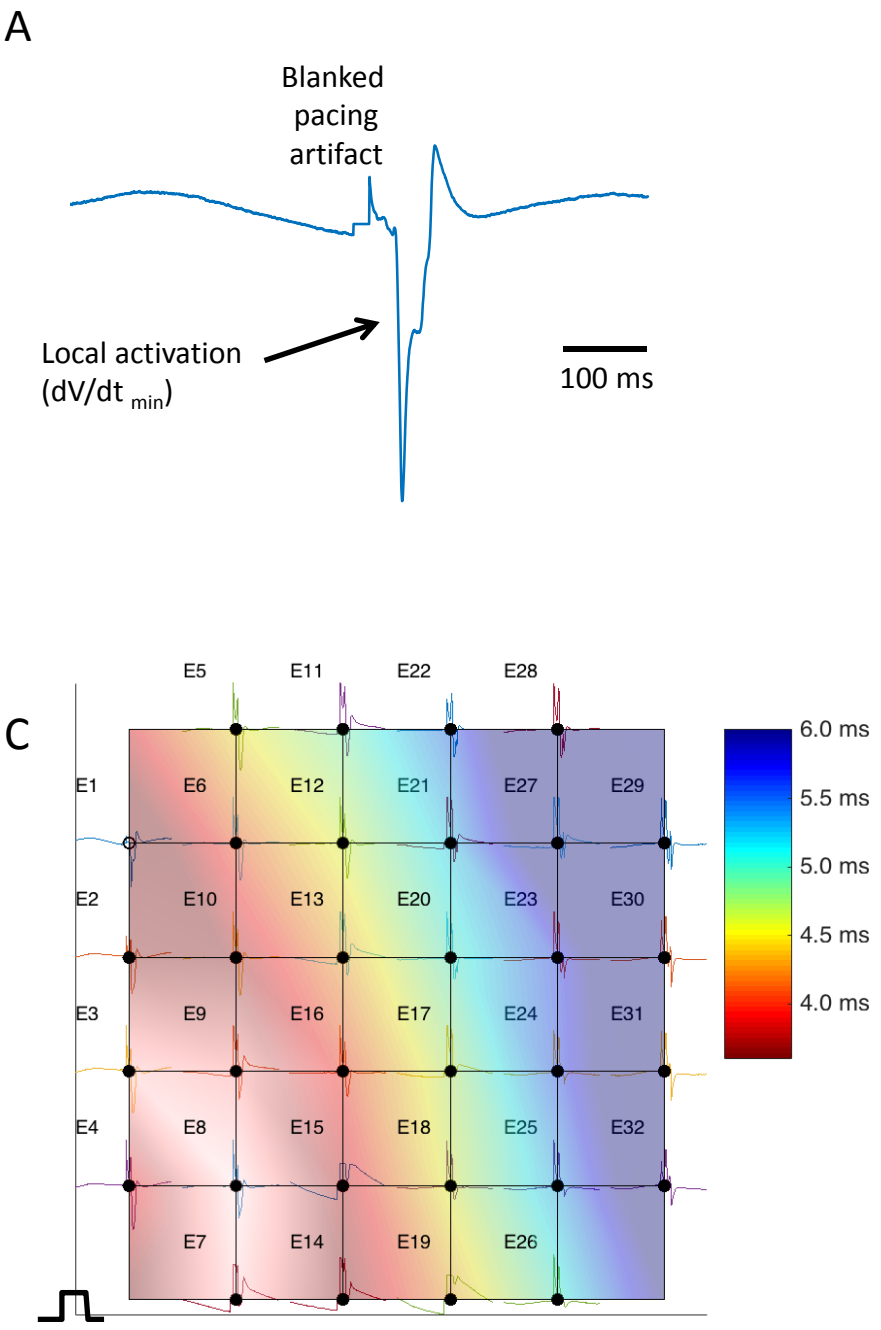
A
Blanked pacing artifact
Local activation (dV/dt min)
100 ms
B
E5 E11 E22 E28
E1 E6 E12 E21 E27 E29
E2 E10 E13 E20 E23 E30
E3 E9 E16 E17 E24 E31
E4 E8 E15 E18 E25 E32
E7 E14 E19 E26
C
E5 E11 E22 E28
E1 E6 E12 E21 E27 E29
E2 E10 E13 E20 E23 E30
E3 E9 E16 E17 E24 E31
E4 E8 E15 E18 E25 E32
E7 E14 E19 E26
6.0 ms
5.5 ms
5.0 ms
4.5 ms
4.0 ms
D
Mean Increase In Delay
Activation Time
Change in Activation Time
Change in Coupling Interval
S1S2 Coupling Interval
18 17 16 15 14 13 12 11 10
70 90 110 130 150 170 190 210

Figure 2

A

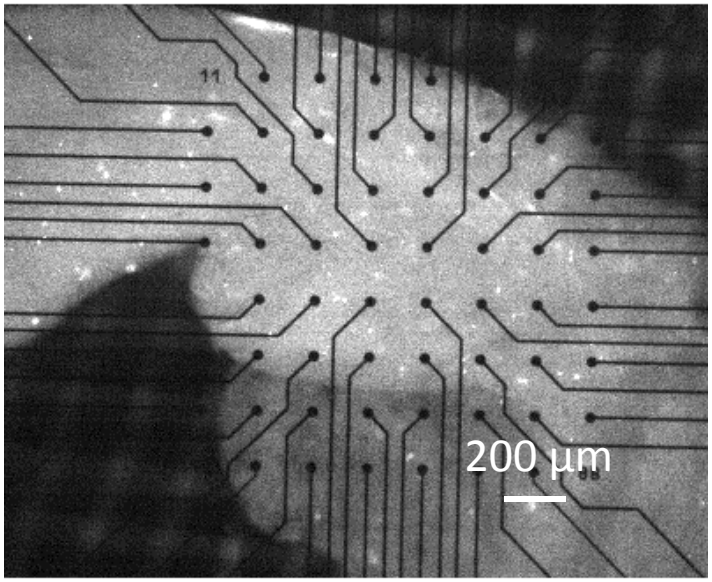

C

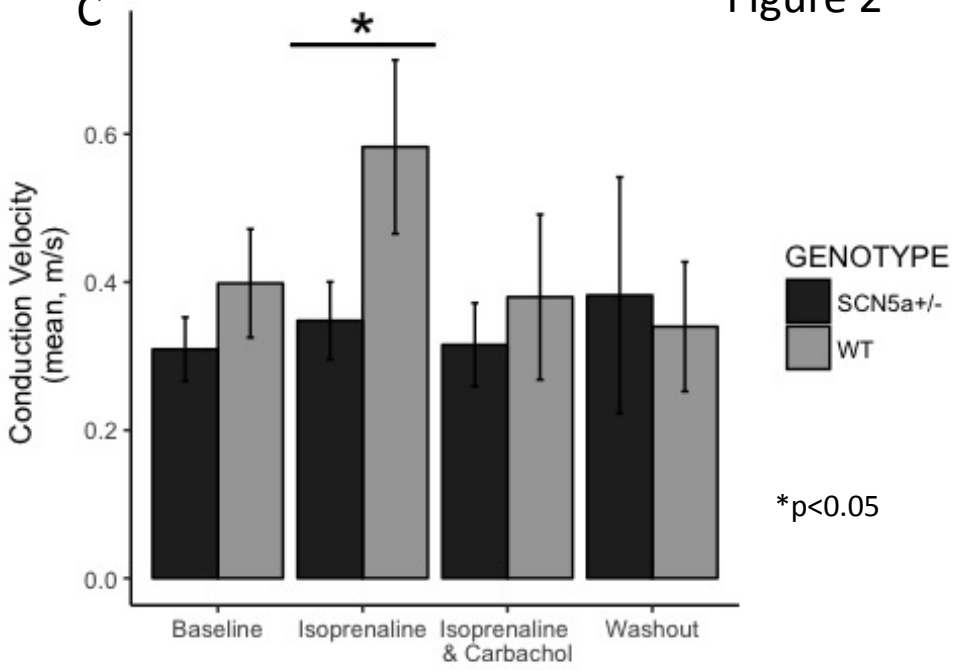

*p<0.05

B

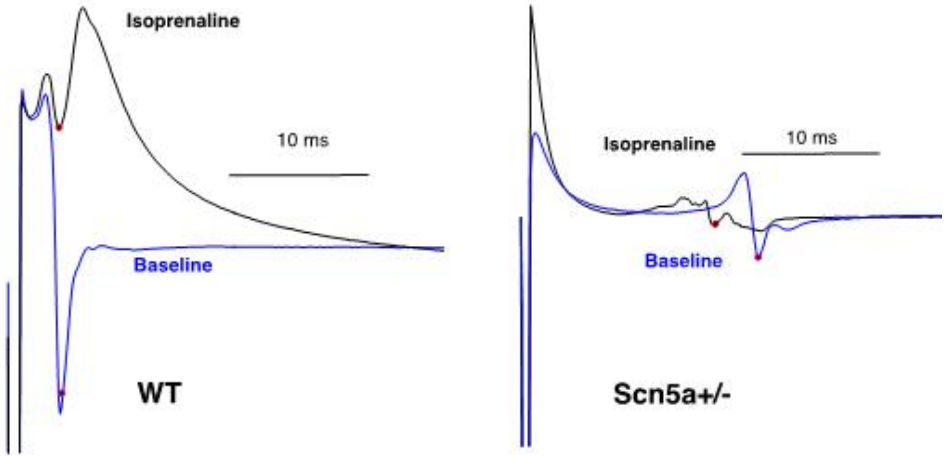

Figure 3

A

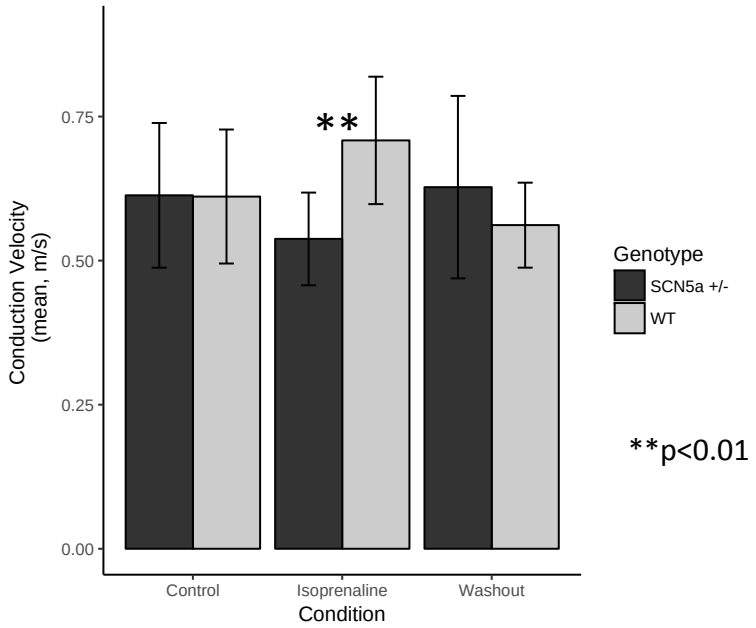

**p<0.01

B

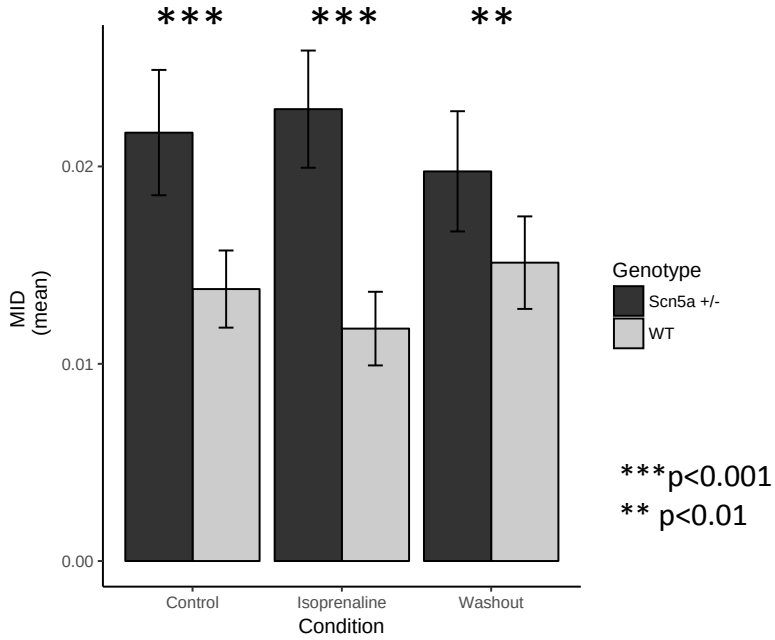

***p<0.001
** p<0.01

C

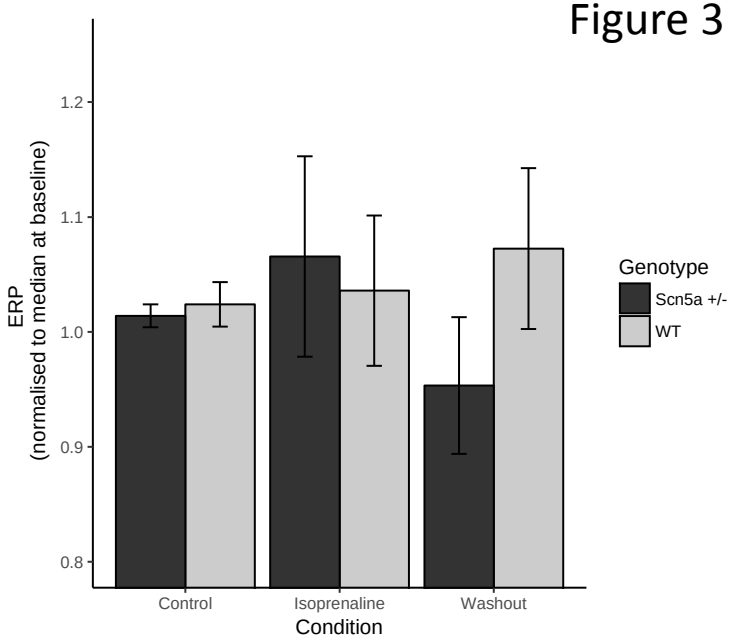

Figure 4

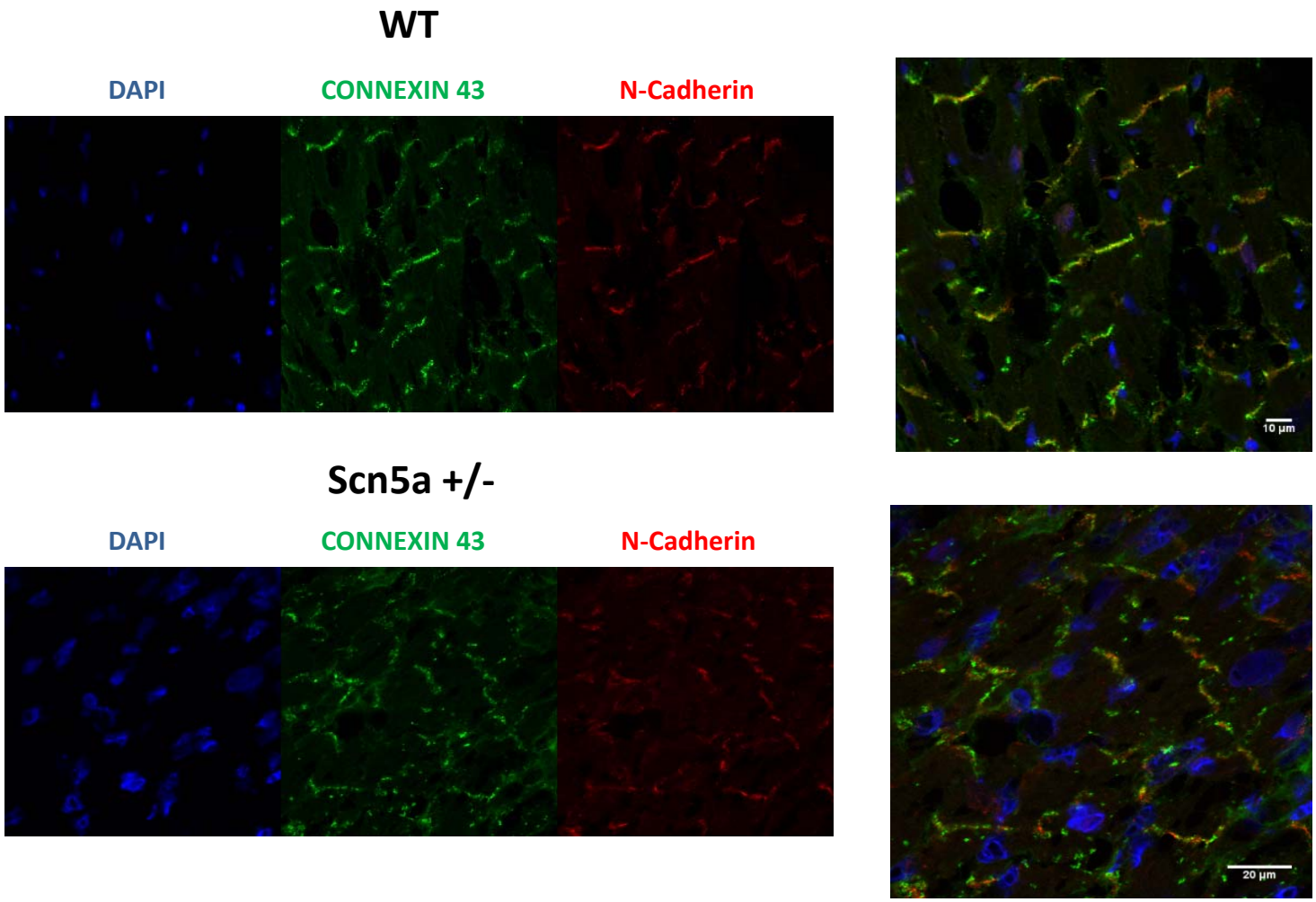
WT
DAPI
CONNEXIN 43
N-Cadherin
10 µm
Scn5a +/-
DAPI
CONNEXIN 43
N-Cadherin
20 µm